Available online at www.sciencedirect.com

SciVerse ScienceDirect

Ceramics International 38 (2012) 1677–1682

CERAMICS INTERNATIONAL

www.elsevier.com/locate/ceramint

Properties of transparent yttrium oxide dielectric films prepared by sol–gel process

Chien-Yie Tsay [a,*], Chia-Hsiang Cheng [a], Yu-Wu Wang [b]

[a] Department of Materials Science and Engineering, Feng Chia University, Taichung 407, Taiwan, ROC
[b] Graduate Institute of Photonics, National Changhua University of Education, Changhua 500, Taiwan, ROC

Received 21 June 2011; received in revised form 20 September 2011; accepted 28 September 2011
Available online 5 October 2011

Abstract

In this research, yttrium oxide (Y_2O_3) gate dielectric films were deposited onto alkali-free glass substrates by a sol–gel process. This report describes the effects of annealing temperatures on the microstructural and electrical properties of sol–gel derived Y_2O_3 films. These sol–gel films were preheated at 300 °C for 10 min, and then annealed at 400–550 °C for 1 h. XRD results revealed that all annealed films exhibited preferential (2 2 2) orientation; films annealed at 450–550 °C were polycrystalline with cubic structures. The average transmittances of polycrystalline Y_2O_3 films were over 88.0% in the visible range. The electrical properties of the Y_2O_3 films were analyzed by capacitance–voltage (*C–V*) and current–voltage (*I–V*) measurements. Films annealed at 500 °C yielded the lowest leakage current density, 1.8×10^{-7} A/cm^2, at an applied voltage of 5 V, and had a dielectric constant of 10.0 at 100 kHz.

Keywords: A. Films; A. Sol–gel processes; C. Dielectric properties; D. Y_2O_3

1. Introduction

Oxide thin film transistors (TFTs) have potential for use in ultra high-definition TFT-LCDs, large-sized 3D displays, active-matrix organic light-emitting device (AMOLED) displays, and flexible displays, because their field-effect mobility and driving currents are higher than those of hydrogenated amorphous silicon (*a*-Si:H) TFTs, and organic TFTs [1–3]. In addition, the oxide TFT fabrication process is simpler than the low-temperature polysilicon (LTPS) TFT process. Recent researches have suggested that both amorphous phase and polycrystalline phase ZnO-based semiconductor might be used to produce low-cost and high-performance TFTs [1,4]. Beside the active channel layer, the gate insulator greatly affects electrical properties of field effect transistors.

An oxide TFT that uses a low-*k* dielectric, such as PECVD SiO_2, as its gate insulator has a small on-current because the low-*k* material has low capacitance [5]. High-*k* dielectrics enable oxide TFTs with low threshold voltages, fast sub-threshold swings, and high field-effect mobility levels. This is because high-*k* materials can increase the physical thickness of gate insulators to prevent electron tunneling and can provide high capacitance values [5,6]. Various high-*k* gate dielectrics (Y_2O_3, Zr_2O_3, HfO_2, $BaSrTiO_3$, etc.) have been used in TFT fabrication to reduce gate leakage currents [7,8].

Yttrium oxide (Y_2O_3) films are not just thermally and chemically stable; they have low leakage current, low dissipation factor, high breakdown voltage, a high *k* constant, and a wide band gap [9]. Various gate dielectrics might be used to product oxide TFTs with outstanding characteristics, but Y_2O_3 is one of the most promising candidate materials [8,10,11]. Hosono et al. reported fabrication of top-gate TFTs with amorphous indium gallium zinc oxide (*a*-IGZO) active layers and Y_2O_3 gate insulators deposited by rf-magnetron sputtering [12]. The TFTs in their study showed a high mobility, 12 cm^2/Vs, and a low sub-threshold swing, 0.2 V/decade. Choi et al. have reported on the electric properties of bottom-gate TFTs, prepared by sputtering, with Y_2O_3 as the gate insulators and *a*-IGZO active layers [6]. The mobility and sub-threshold swing of their TFTs were 6.9 cm^2/Vs and 0.3 V/decade. Quite recently, G. Adamopoulos et al. reported ZnO TFTs based on spray pyrolysed Y_2O_3 dielectrics show low leakage currents

* Corresponding author. Tel.: +886 4 24517250x5312; fax: +886 4 24510014.
E-mail address: cytsay@fcu.edu.tw (C.-Y. Tsay).

0272-8842/$36.00
doi:10.1016/j.ceramint.2011.09.060

and hysteresis-free operation with a mobility of 34 cm^2/Vs [8]. Moreover, Y_2O_3 films have been used as the charge-trapping layer of nonvolatile memory [13,14].

The fabrication of oxide TFTs resembles vacuum deposition processes such as physical vapor deposition (PVD). Solution-based deposition processes are simple and cost-effective, and can coat a large area with a thin film; solution-based deposition processes offer an alternative to vacuum deposition techniques [15,16]. Preparation of gate dielectrics by solution-based processes such as the sol–gel process may reduce equipment costs, and may increase the smoothness and uniformity of the films' surfaces [17]. In an inverted staggered TFT, the gate insulator is thick (200–300 nm) for adequate step coverage at the gate edge [18]. Sol–gel derived metal oxide dielectrics can provide good step coverage for the gate metals as well as can offer the possibility of direct patterning of gate insulators.

In the present study, transparent Y_2O_3 dielectric films were prepared by the sol–gel method using a spin-coating technique. The authors investigated the effects of annealing temperatures on the structures, optical transparency levels and electrical properties of Y_2O_3 dielectric films. The authors measured capacitance–voltage (*C–V*) and leakage current–voltage (*I–V*) to analyze the film's electrical properties. Moreover, the leakage current conduction mechanism for ITO/Y_2O_3/Al capacitors was discussed in the present study.

2. Experimental procedures

The precursor solution of yttrium oxide was synthesized by the following steps. First, yttrium (III) acetate tetrahydrate (Alfa Aesar, 99.99%) was dissolved in 2-methoxyethanol (2-ME, Alfa Aesar, 99.9%), and then diethanolamine (DEA, J.T. Baker, 99.9%) was added to the mixed solution as a stabilizer. The resultant solution was stirred for 1 h at 60 °C, and then aged for 10 days to yield a homogeneous sol. The molar ratio of yttrium ions to DEA in the as-prepared sol was maintained at 1:2, and the yttrium ions concentration was controlled at 0.4 mole/L. Each yttrium oxide gel film was spin-coated onto alkali-free glass substrates (OA-10 from Nippon Electric Glass Co., Ltd.) at a speed of 1000 rpm for 30 s. These as-coated films were preheated at 300 °C for 10 min. After the spin-coating and preheating procedures had been repeated three times, the films were annealed at various temperatures (400–550 °C) for 1 h under air ambiance in a quartz tube furnace.

Thermogravimetric analysis (TGA) and differential scanning calorimetry (DSC) curves of the yttrium oxide precursor solution were recorded using a TA Instruments SDT 2960 thermal analyzer. The crystal structures of annealed yttrium oxide films were determined by a Bruker D8 SSS high-resolution X-ray diffractometer (HRXRD) with Cu Kα radiation. Cross-sectional micrographs of yttrium oxide films were observed by a Hitachi S-4800 field-emission scanning electron microscope (FE-SEM). The surface roughness levels of the films were measured by an automated atomic force microscopy (AFM, NT-MDT Solver P7LS, Russia). The optical transmittance spectra of the films were recorded with a Hitachi U-2900 UV–VIS spectrophotometer.

ITO (100 nm)/Y_2O_3 (220 ± 5 nm)/Al (100 nm) stacked structures were formed on glass substrates for examining the electrical properties of Y_2O_3 films. First, Y_2O_3 films were deposited onto the ITO glass substrate, and then Al top electrodes were deposited on Y_2O_3 films by thermal evaporation through a stainless steel shadow mask that measured 1 mm × 1 mm. The capacitance–voltage (*C–V*) and current–voltage (*I–V*) curves of the ITO/Y_2O_3/Al capacitors were measured by means of an Agilent E4980A LCR meter and a Keithley 2636A sourcemeter, respectively.

3. Results and discussion

Thermal analysis results determined from TGA and DSC, as shown in Fig. 1, were used to identify the evaporation, decomposition, and crystallization characteristics of the yttrium oxide precursor solution. In the TGA curve, weight loss was observed for three temperature regions at 50–95 °C, 110–330 °C, and 370–450 °C. Since the boiling point of the solvent 2-ME is 124 °C, and the decomposition temperatures of DEA and yttrium acetate are 268 °C and 285 °C. The first and second weight loss regions were caused by evaporation of solvent and water, and by decomposition of DEA and yttrium acetate; the third weight loss region was resulted from decomposition of residual organic compounds. Moreover, no weight loss occurred in the TGA curve when the precursor solution was heated at temperatures above 470 °C; this indicated the absence of organic compounds. The DSC curve shows a large endothermic peak and a large exothermic peak. The endothermic peak at 90 °C can be ascribed to abrupt solvent evaporation of yttria sol; the exothermic peak at 378 °C and a shoulder at 445 °C can be associated with thermo-oxidative combustion of residual organics and of Y_2O_3 film crystallization [19,20].

X-ray diffraction patterns of Y_2O_3 films annealed at different temperatures and the corresponding pattern of the preheated film are shown in Fig. 2. XRD spectrum of preheated film

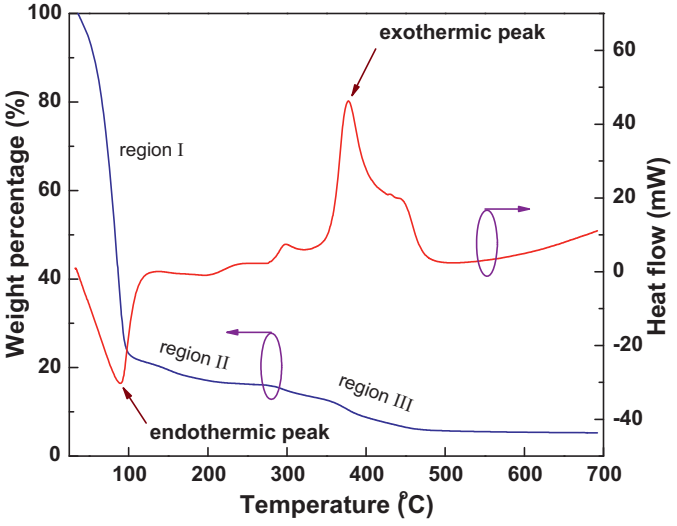

Fig. 1. TGA and DSC curves measured under air ambiance at a heating rate of 10 °C/min for yttrium oxide precursor solution.

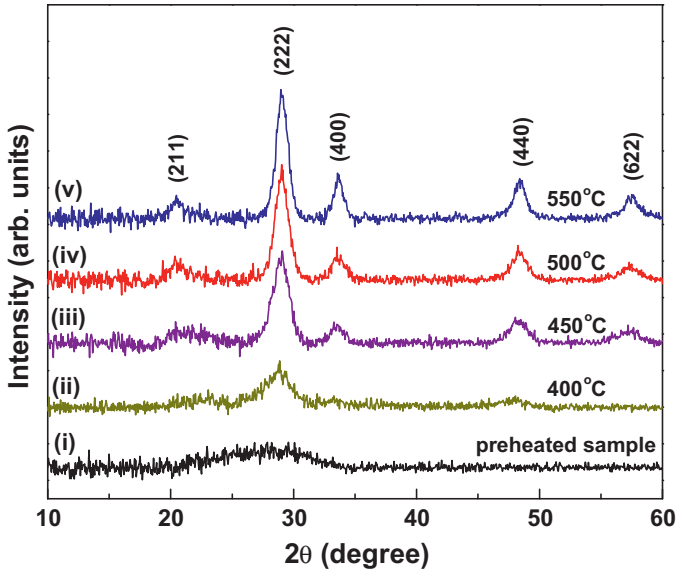

Fig. 2. X-ray diffraction patterns of the preheated film and Y_2O_3 films with various annealing temperatures.

shows a weak and broad diffraction signal (curve (i) in Fig. 2); that curve indicates that the film was amorphous or had a nanocrystalline phase. XRD results also show that all annealed Y_2O_3 films had a strong preferential orientation along the (2 2 2) plane (curves (ii)–(v) in Fig. 2). The diffraction patterns of Y_2O_3 films annealed at 450–550 °C corresponded to five diffraction peaks of polycrystalline Y_2O_3 (JCPDS 89-55921); thus, three annealed films had a cubic bixbyite structure (curves (iii)–(v) in Fig. 2). The intensities of all diffraction peaks had a tendency to increase as annealing temperatures increased from 450 to 550 °C; the full width at half maximum (FWHM) for the diffraction peaks of corresponding films decreased as annealing temperatures increased. The crystallite sizes of the films were estimated with Scherrer's formula [21]. The average crystallite sizes for the three main diffraction peaks of the (2 2 2), (4 0 0),

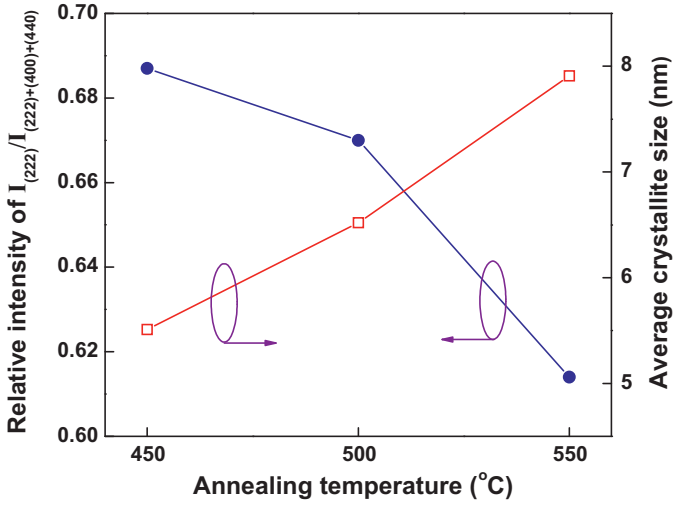

Fig. 3. Variation of relative intensity of $I_{(2\,2\,2)}/I_{(2\,2\,2)+(4\,0\,0)+(4\,4\,0)}$ and average crystallite size for Y_2O_3 films with annealing temperature.

and (4 4 0) planes of films annealed at 450, 500, and 550 °C were 5.5, 6.5, and 7.9 nm, respectively. Fig. 3 shows that the crystallite size averages increased as annealing temperature increased. These results indicate that high annealing temperatures enhanced crystallization and increased average crystallite sizes.

XRD results indicate that the annealed Y_2O_3 films began to crystallize at 400 °C (curve (ii) in Fig. 2); that result confirms prior finding concerning films deposited by e-beam evaporation [20]. A sol–gel derived Y_2O_3 film tends to exhibit its strongest (2 2 2) orientation when its (2 2 2) plane has the lowest possible surface energy [9]. In this research, the diffraction peaks of the (2 1 1), (4 0 0), (440), and (6 2 2) planes were observed as the annealing temperature was raised to 450 °C. Fig. 3 shows how the relative intensity of $I_{(2\,2\,2)}/I_{(2\,2\,2)+(4\,0\,0)+(4\,4\,0)}$ varied with annealing temperature. It can be seen that the relative intensity of $I_{(2\,2\,2)}/I_{(2\,2\,2)+(4\,0\,0)+(4\,4\,0)}$ decreased as annealing temperature increased. A higher annealing temperature supplies higher kinetic energy and increases the mobility of deposited atoms that contribute to grain growth [22].

Cross-sectional SEM micrographs of annealed Y_2O_3 films are shown in Fig. 4. These SEM images reveal that all annealed Y_2O_3 films had flat surfaces; films annealed at 450–550 °C were polycrystalline and exhibited granular structures. The average thicknesses for films annealed at 400, 450, 500, and 550 °C were about 300 nm, 225 nm, 220 nm, and 220 nm, respectively (Fig. 4(a)–(d)). Fig. 4(a) and (b) shows that a preheated film annealed at 400 °C had a thickness 300 nm but that a similar preheated film annealed at 450 °C had a starkly different thickness, 225 nm. This was due to decomposition of residual organic compounds and greater crystallization for films annealed at temperatures ≥450 °C. Moreover, SEM micrographs (Fig. 4(c) and (d)) for films annealed at 500 and 550 °C show dense structures. Those dense structures can be ascribed to the high annealing temperatures that enhanced crystallization and grain size growth.

The relationship of root mean square (RMS) roughness to annealing temperature is shown in Fig. 5 that reveals RMS roughness increased from 0.20 to 0.38 nm as annealing temperature increased from 450 to 550 °C. This tendency corresponds to the relationship of average crystallite size to annealing temperature. The inset of Fig. 5 shows optical transmittance spectra of Y_2O_3 films with wavelengths from 350 to 850 nm. The optical transmittance percentage in the visible region depends on the wavelengths. The average transmittance values for these films were over 88.0%. Thus, these sol–gel derived Y_2O_3 dielectric films were transparent materials, which could be considered for transparent TFTs.

Fig. 6 shows the capacitance-voltage (*C–V*) characteristics of ITO/Y_2O_3/Al capacitors that were measured at a frequency of 100 kHz; for each capacitor, applied DC voltage was swept from −10 to 10 V. The average capacitance density increased from 37.4 nF/cm^2 at an annealing temperature of 450 °C to 42.2 nF/cm^2 at 550 °C. Fig. 6 also shows the slight instability of *C–V* characteristics for 500 and 550 °C samples. The trapping/detrapping of electrons caused non-constant *C–V* characteristics [23]. The dielectric constants (ε_r) of sol–gel derived Y_2O_3

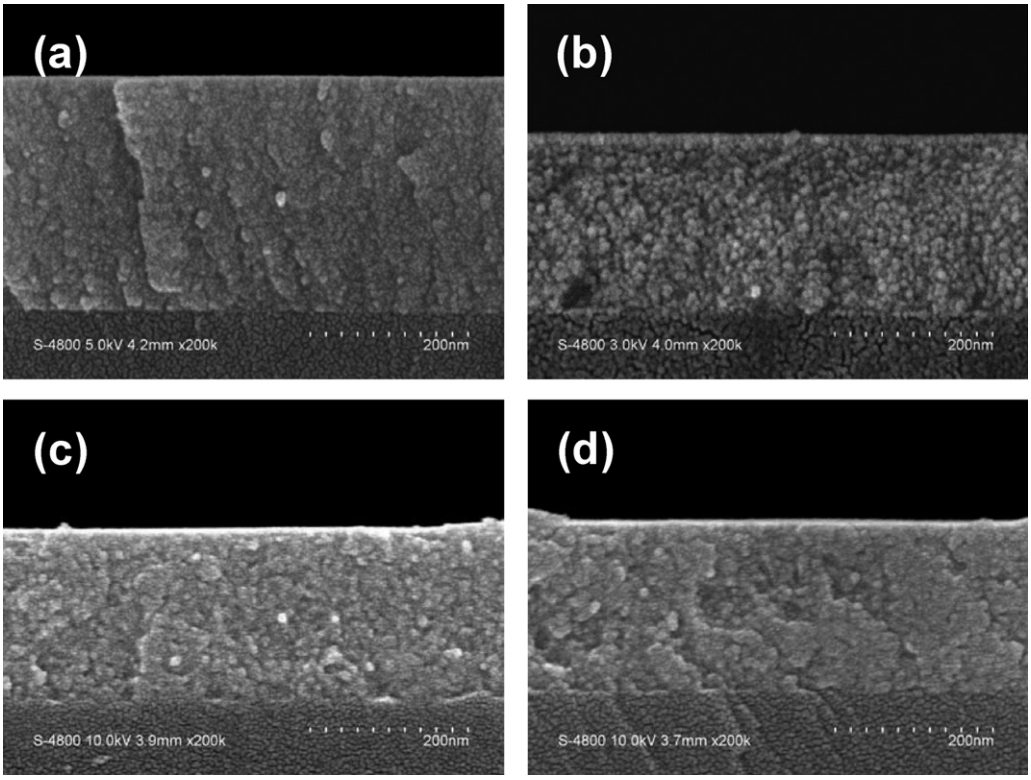

Fig. 4. Cross-sectional SEM photographs of Y_2O_3 films annealed at different temperatures: (a) 400 °C, (b) 450 °C, (c) 500 °C, and (d) 550 °C.

films were calculated from the following relation,

$$\varepsilon_r = \frac{Cd}{\varepsilon_0 A} \quad (1)$$

where absolute permittivity $\varepsilon_0 = 8.8542 \times 10^{-12}$ C/Vm, and C, d, and A are the capacitance for ITO/Y_2O_3/Al stacked structure, the thickness of Y_2O_3 film, and the area of top electrode. The calculated dielectric constants for films annealed at temperatures of 450, 500, and 550 °C were 9.5, 10.0, and 10.5, respectively. That result reveals dielectric constant increased as annealing temperature increased. This happened because the films' dielectric constants related to grain sizes and degrees of crystallization [22]. Moreover, the dielectric constant values of these films were smaller than bulk ($\varepsilon_r = 18$) [20] and sputtered films ($\varepsilon_r = 16$) values [6] because of the relatively low densities and fine grain sizes of the sol–gel derived Y_2O_3 films.

Fig. 7 shows the current density–voltage (J–V) characteristics of ITO/Y_2O_3/Al capacitors. The ITO/Y_2O_3/Al capacitors had symmetric J–V curves. Fig. 7 also shows that no significant breakdown behavior was observed in all samples, and that the

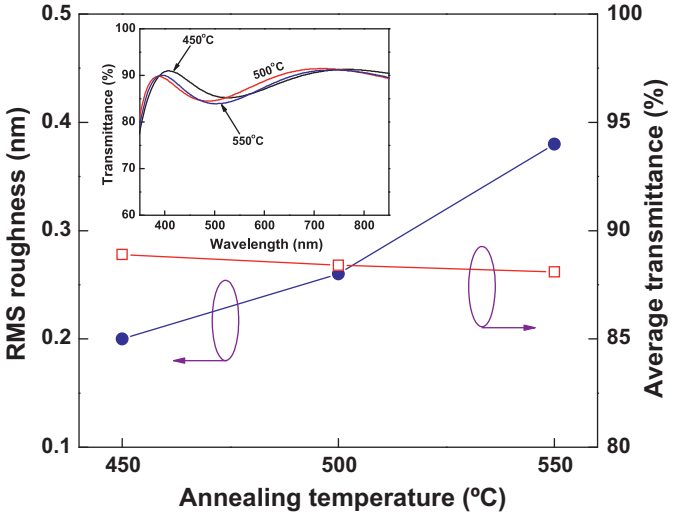

Fig. 5. Variation of RMS roughness and average transmittance for Y_2O_3 films with annealing temperature. The inset plot shows optical transmittance spectra for Y_2O_3 films.

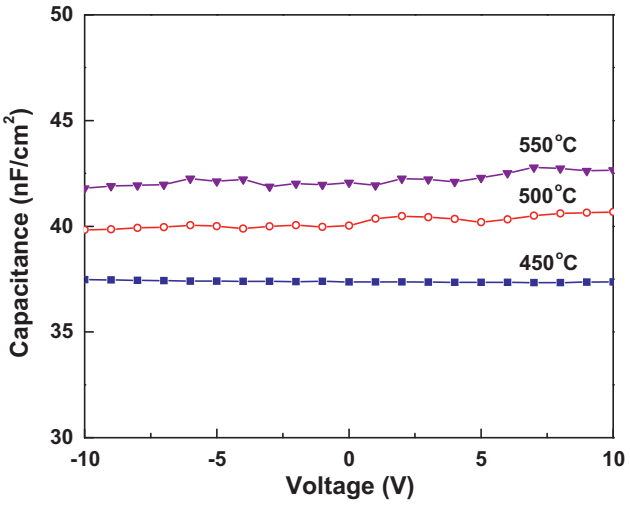

Fig. 6. Capacitance–voltage (C–V) characteristics of ITO/Y_2O_3/Al capacitors.

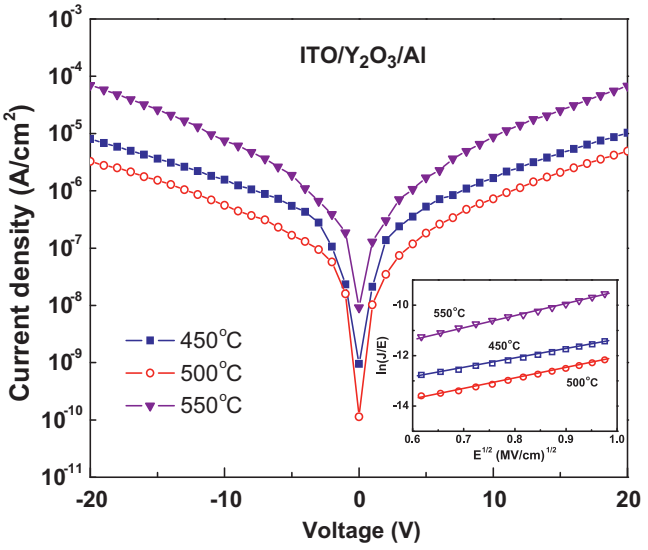

Fig. 7. Current density–voltage (J–V) characteristics of ITO/Y_2O_3/Al capacitors. The inset shows the Poole–Frenkel emission plot of ln(J/E) versus $E^{1/2}$ according to J–V data.

samples annealed at 500 °C exhibited the best insulating properties. A film's leakage current characteristics are affected by microstructure, crystallinity, and surface roughness [22,24]. Annealing of the Y_2O_3 film at high temperatures (500–550 °C) reduces intrinsic defects, increases crystallization, and reduces grain boundaries. However, samples annealed at 550 °C showed a high leakage current density of 1.7×10^{-6} A/cm^2 at an applied voltage of 5 V. It is possible inter-diffusion between the Y_2O_3 and ITO films may occur during samples annealed at 550 °C. That behavior leads to reduce physical thickness of dielectric film and causes to increase the leakage current. Moreover, the heat treatment temperature of 550 °C might have been close to the glass transition temperature (T_g) of glass substrates that it might have induced internal stresses in the films. Films annealed at 500 °C yielded the lowest leakage current density of 1.8×10^{-7} A/cm^2 at 5 V; those films exhibited more insulating behavior than solution-processed SiO_2 films [25,26].

Several current conduction models have been used to explain the I–V characteristics of metal/insulator/metal (M/I/M) stacked structures [27]. In general, the J–V characteristics of dielectric films appear to follow typical Schottky emission and Poole–Frenkel emission. If the Poole–Frenkel model dominates current transport, then ln(J/E) is a linear function of the square root of the electric field (E). The inset of Fig. 7 plots the Poole–Frenkel emission plot of ln(J/E) versus $E^{1/2}$ according to J–V data; this inset indicates the leakage current conduction mechanism in ITO/Y_2O_3/Al capacitors was dominated by Poole–Frenkel emission under electric fields between 0.35 and 0.95 MV/cm.

4. Conclusions

Transparent yttrium oxide gate dielectric films have been prepared by a sol–gel spin coating process. All annealed films exhibited a preferred orientation along the [2 2 2] direction, and films annealed at 450–550 °C had a cubic bixbyite structure. These polycrystalline Y_2O_3 films were highly transparent, with average transmittances exceeding 88.0% for wavelengths between 350 and 850 nm. Among the sol–gel derived Y_2O_3 dielectric films in this study, the films annealed at 500 °C exhibited a dielectric constant of 10.0 at 100 kHz, and the lowest leakage current density, namely 1.8×10^{-7} A/cm^2 at 5 V. The leakage current conduction mechanism was dominated by Poole–Frenkel emission.

Acknowledgments

The authors gratefully acknowledge the financial support of the National Science Council of the Republic of China under contract number NSC 99-2221-E-035-034-MY3.

References

[1] R.A. Street, Thin-film transistors, Adv. Mater. 21 (2009) 2007–2022.
[2] S.-H.K. Park, C.-S. Hwang, M. Ryu, S. Yang, C. Byun, J. Shin, J.-I. Lee, K. Lee, M.S. Oh, S. Im, Transparent and photo-stable ZnO thin-film transistors to drive an active matrix organic-light-emitting-diode display panel, Adv. Mater. 21 (2009) 678–682.
[3] K. Nomura, H. Ohta, A. Takagi, T. Kamiya, M. Hirano, H. Hosono, Room-temperature fabrication of transparent flexible thin-film transistors using amorphous oxide semiconductors, Nature 432 (2004) 488–492.
[4] J.K. Jeong, The status and perspectives of metal oxide thin-film transistors for active matrix flexible displays, Semicond. Sci. Technol. 26 (2011) 034008.
[5] Y.S. Chun, S. Chang, S.Y. Lee, Effects of gate insulators on the performance of a-IGZO TFT fabricated at room-temperature, Microelectron. Eng. 88 (2011) 1590–1593.
[6] Y.J. Cho, J.H. Shin, S.M. Bobade, Y.B. Kim, D.K. Choi, Evaluation of Y_2O_3 gate insulators for a-IGZO thin film transistors, Thin Solid Films 517 (2009) 4115–4118.
[7] S.Y. Lee, S. Chang, J.S. Lee, Role of high-k gate insulators for oxide thin film transistors, Thin Solid Films 518 (2010) 3030–3032.
[8] G. Adamopoulos, S. Thomas, D.D.C. Bradley, M.A. McLachlan, T.D. Anthopoulos, Low-voltage ZnO thin-film transistors based on Y_2O_3 and Al_2O_3 high-k dielectrics deposited by spray pyrolysis in air, Appl. Phys. Lett. 98 (2011) 123503.
[9] G. Teowee, K.C. McCarthy, F.S. McCarthy, T.J. Bukowski, D.G. Davis Jr., D.R. Uhlmann, Preparation and characterization of sol–gel derived Y_2O_3 thin films, J. Sol–Gel Sci. Technol. 13 (1998) 895–898.
[10] P.S. Das, G.K. Dalapati, D.Z. Chi, A. Biswas, C.K. Maiti, Characterization of Y_2O_3 gate dielectric on n-GaAs substrates, Appl. Surf. Sci. 256 (2010) 2245–2251.
[11] S.M. Bobade, J.H. Shin, Y.J. Cho, J.S. You, D.K. Choi, Room temperature fabrication oxide TFT with Y_2O_3 as a gate oxide and Mo contact, Appl. Surf. Sci. 255 (2009) 7831–7833.
[12] H. Yabuta, M. Sano, K. Abe, T. Aiba, T. Den, H. Kumomi, K. Nomura, T. Kamiya, H. Hosono, High-mobility thin-film transistor with amorphous $InGaZnO_4$ channel fabricated by room temperature rf-magnetron sputtering, Appl. Phys. Lett. 89 (2006) 112123.
[13] T.M. Pan, W.W. Yeh, A high-k Y_2O_3 charge trapping layer for nonvolatile memory application, Appl. Phys. Lett. 92 (2008) 173506.
[14] C.M. Lin, W.C. Shih, Y.K. Chang, P.C. Juan, Y.M. Lee, Metal-ferroelectric, ($BiFeO_3$)-insulator (Y_2O_3)-semiconductor capacitors and field effect transistors for nonvolatile memory applications, Appl. Phys. Lett. 94 (2009) 142905.
[15] K.K. Banger, Y. Yamashita, K. Mori, R.L. Peterson, T. Leedham, J. Rickard, H. Sirringhaus, Low-temperature, high-performance solution-processed metal oxide thin-film transistors formed by a 'sol–gel on chip' process, Nat. Mater. 10 (2011) 45–50.

[16] M.G. Kim, M.G. Kanatzidis, A. Facchetti, T.J. Marks, Low-temperature fabrication of high-performance metal oxide thin-film electronics via combustion processing, Nat. Mater. 10 (2011) 382–388.
[17] S.J. Kim, G.H. Kim, D.L. Kim, D.N. Kim, H.J. Kim, InGaZnO thin-film transistors with YHfZnO gate insulator by solution process, Phys. Status Solidi A 207 (2010) 1668–1671.
[18] T. Tsukada, TFT/LCD: Liquid–Crystal Displays Addressed by Thin-Film Transistors, Gordon and Breach, The Netherlands, 1996.
[19] G.A.M. Hussein, Formation of high surface-area yttrium oxide by the thermal decomposition of different inorganic precursors, Thermochim. Acta 244 (1994) 139–151.
[20] A.C. Rastogi, R.N. Sharma, Structural and electrical characteristics of metal-insulator–semiconductor diodes based on Y_2O_3 dielectric thin films on silicon, J. Appl. Phys. 71 (1992) 5041–5052.
[21] B.D. Cullity, S.R. Stock, Elements of X-ray Diffraction, 3rd ed., Prentice-Hall Inc., New Jersey, 2001.
[22] C.H. Hsu, S.F. Yan, Fabrication and characterization of $ZnNb_2O_6$ thin films using sol–gel method, J. Am. Ceram. Soc. 94 (2011) 822–826.
[23] B.Y. Tsui, H.H. Hsu, C.H. Cheng, High-performance metal-insulator-metal capacitors with $HfTiO/Y_2O_3$ stacked dielectric, IEEE Electron Device Lett. 31 (2010) 875–877.
[24] Y.P. Zhao, G.C. Wang, T.M. Lu, G. Palasantzas, J.Th.M. De Hosson, Surface-roughness effect on capacitance and leakage current of an insulating film, Phys. Rev. B 60 (1999) 9157–9164.
[25] S.B. Jung, H.H. Park, H. Kim, Investigation of the bonding states of the SiO_2 aerogel film/metal interface, Thin Solid Films 447–448 (2004) 575–579.
[26] J. Kákoš, M. Mikula, L. Harmatha, Ultrathin insulating silica layers prepared from adsorbed TEOS, H_2O and NH_3 as a catalyst, Microelectron. J. 39 (2008) 1626–1628.
[27] S.M. Sze, Physics of Semiconductor Devices, 2nd ed., John Wiley & Sons, New York, 1981.